THE JOURNAL OF BIOLOGICAL CHEMISTRY VOL. 280, NO. 50, pp. 41307–41314, December 16, 2005

Stability Domains, Substrate-induced Conformational Changes, and Hinge-bending Motions in a Psychrophilic Phosphoglycerate Kinase

*A MICROCALORIMETRIC STUDY**

Received for publication, June 14, 2005, and in revised form, October 14, 2005 Published, JBC Papers in Press, October 14, 2005, DOI 10.1074/jbc.M506464200

Laurent Zecchinon, Annick Oriol, Ulrike Netzel, Julie Svennberg, Nicole Gerardin-Otthiers, and Georges Feller[1]

From the Laboratory of Biochemistry, University of Liège, Institute of Chemistry B6a, B-4000 Liège-Sart Tilman, Belgium

The cold-active phosphoglycerate kinase from the Antarctic bacterium *Pseudomonas* sp. TACII18 exhibits two distinct stability domains in the free, open conformation. It is shown that these stability domains do not match the structural N- and C-domains as the heat-stable domain corresponds to about 80 residues of the C-domain, including the nucleotide binding site, whereas the remaining of the protein contributes to the main heat-labile domain. This was demonstrated by spectroscopic and microcalorimetric analyses of the native enzyme, of its mutants, and of the isolated recombinant structural domains. It is proposed that the heat-stable domain provides a compact structure improving the binding affinity of the nucleotide, therefore increasing the catalytic efficiency at low temperatures. Upon substrate binding, the enzyme adopts a uniformly more stable closed conformation. Substrate-induced stability changes suggest that the free energy of ligand binding is converted into an increased conformational stability used to drive the hinge-bending motions and domain closure.

Phosphoglycerate kinase (PGK[2]; EC 2.7.2.3) catalyzes the reversible high energy phosphoryl transfer from 1,3-diphospho-D-glycerate to Mg^{2+}-ADP to yield Mg^{2+}-ATP and 3-phospho-D-glycerate (3-PGA) in the glycolytic pathway. Besides its key metabolic function in living organisms, PGK has been widely used as a model enzyme to study domains in proteins and their relative motions (1, 2). Indeed, the structure of PGK consists of two globular domains of nearly equal size, referred to as the N- and C-terminal domains, linked by a hinge helix. In this structure, the C terminus of the protein crosses back the hinge region and folds into the N-domain, bringing the N- and C-extremities in close proximity where they generally interact via ion pairs (3, 4). The triose substrate binds to a basic patch in the N-domain (5), whereas the nucleotide substrate is bound to the C-domain (6). Crystallographic studies have shown that the free or single substrate-liganded forms adopt an open conformation in which the distance between the substrates is too long to permit catalysis, probably to avoid the futile hydrolysis of 1,3-PGA or ATP (7). By contrast, the binding of both substrates induces a closed conformation resulting from hinge-bending motions of 32° at the level of the hinge helices and leading to domain closure into a catalytically competent conformation with well aligned substrates for phosphoryl transfer (7, 8).

The stability and folding of yeast PGK has been extensively investigated and deconvolution of its single DSC heat absorption peak suggests the occurrence of two overlapping transitions that have been tentatively assigned to the N- and C-domains (9). Furthermore, folding studies using guanidinium chloride as denaturation agent have suggested that the C-domain is the most stable domain, although contradicting results have been reported (9–13). In this context, the PGK from the Antarctic bacterium *Pseudomonas* sp. TACII18 (*Ps*PGK) represents a unique model to study stability domains in PGK. The high level of amino acid sequence similarity of *Ps*PGK with phosphoglycerate kinases from other species has allowed the building of a homology model based on the available crystal structures (14). Furthermore, crystals of *Ps*PGK have been obtained (15), and its structure solved at 2.1 Å resolution indeed reveals a general fold identical to that of other monomeric PGKs.[3] However, the preliminary characterization of *Ps*PGK by DSC (14) has shown that it possesses two well defined transitions in the unliganded conformation (see also Fig. 1). It follows that the enzyme contains two types of structures or regions differing by their intrinsic stability and responsible for the occurrence of a heat-labile domain (melting point (T_m) ~50 °C) and a heat-stable domain (T_m ~60 °C) when thermal unfolding is recorded by DSC. Such stability domains within the protein may or may not correspond to the structural N- and C-domains. One cannot exclude for instance that each structural domain contains both heat-labile and heat-stable structures that unfold sequentially. We report here the unusual stability pattern of this enzyme and the complex effects of substrate binding inducing hinge-bending motions. The results have several implications in folding studies of PGK and of proteins in general as well as in the field of enzyme adaptations to extreme temperatures.

EXPERIMENTAL PROCEDURES

Mutagenesis of PsPGK—The *pgk* gene from the Antarctic bacterium *Pseudomonas* sp. TACII18 has been cloned in the expression vector pET22b as previously described (14). Genetic engineering was performed on the gene or on gene fragments inserted in the plasmid pSP73. Mutations were introduced by polymerase chain reaction as described (16). The mutation $Trp^{305} \rightarrow Phe$ was introduced by changing the codon TGG into TTC on the gene fragment generated by SalI-PstI digestion. The mutation $Phe^{135} \rightarrow Trp$ was introduced by changing the codon TTT into TGG on the gene fragment generated by XbaI-SalI digestion. Deletion of domain coding regions was carried out by inverse PCR using silent primers, 24 nucleotides in length, starting in 5′ at codon for Thr^{1} (reverse primer) and for Ala^{172} (forward primer) for the

* This work was supported by the Fonds National de la Recherche Scientifique, Belgium (Grants FRFC 2.4515.00 and 2.4536.04). The costs of publication of this article were defrayed in part by the payment of page charges. This article must therefore be hereby marked "*advertisement*" in accordance with 18 U.S.C. Section 1734 solely to indicate this fact.

[1] To whom correspondence should be addressed. Tel.: 32-4-366-33-43; Fax: 32-4-366-33-64; E-mail: gfeller@ulg.ac.be.

[2] The abbreviations used are: *Ps*PGK, phosphoglycerate kinase from *Pseudomonas* sp. TACII18; DSC, differential scanning calorimetry; 3-PGA, 3-phospho-D-glycerate; AMP-pnp, 5′-adenylylimidodiphosphate; Mops, 3-(*N*-morpholino)propanesulfonic acid.

[3] D. Mandelman, D. A. Wolff, G. Feller, C. Gerday, R. Haser, and N. Aghajari, manuscript in preparation.

deletion of the N-domain and starting in 5′ at codon for Leu^{170} (reverse primer) and at the stop codon (forward primer) for the deletion of the C-domain. The amplification products were purified (QIAquick PCR purification kit, Qiagen), phosphorylated by T4 polynucleotide kinase and circularized by ligation before transformation. The sequence of these constructions was checked by double-strand sequencing on an ALF DNA sequencer Express II (Amersham Biosciences) and transferred to the expression vector using appropriate restriction sites.

Protein Expression and Purification—The recombinant proteins were expressed in *Eschericha coli* BL21(DE3) grown at 18 °C as described previously (14), except that Terrific broth was used for cultivation and induction with 0.5 mM isopropyl 1-thio-β-galactopyranoside was performed at $A_{600\,nm}$ of the culture between 3 and 5. The recombinant proteins were purified essentially as described (14) following high pressure or freeze-thawing cell disruption, protamine sulfate precipitation of nucleic acids, ammonium sulfate fractionation, phenyl-Sepharose, and Q-Sepharose chromatography. The double mutant $Phe^{135} \rightarrow Trp/Trp^{305} \rightarrow Phe$ was precipitated at 50% ammonium sulfate saturation, whereas the recombinant isolated domains were brought to 30% ammonium sulfate saturation before phenyl-Sepharose chromatography. For the domain proteins, the buffer was 50 mM Tris, 0.5 mM EDTA, 5 mM dithiothreitol, 0.1 mM benzamidine, pH 7.5, and a second Q-Sepharose chromatography was required. All the proteins were pure on the basis of a single band on SDS-PAGE, a single N-terminal amino acid sequence, and a single ion distribution in mass spectrometry.

Analytical Procedures—N-terminal amino acid sequences were determined using a pulsed liquid-phase protein sequencer (Procise 492, Applied Biosystems, PerkinElmer Division) fitted with an on-line phenylthiohydantoin analyzer. Electrospray mass spectrometry of the proteins (5–10 μM) was performed on a Q-TOF Ultima mass spectrometer (Micromass). Absorbance spectra were recorded on an Uvikon XS spectrophotometer (Bio-Tek Instruments). Fluorescence spectra were recorded on an SLM-Aminco model 8100 spectrofluorimeter (Spectronic Instruments). Circular dichroism spectra were acquired under constant nitrogen flush using a J-810 spectropolarimeter (Jasco Corp.) in a 0.2-cm path length cell for the far-UV region. All spectrophotometric analyses were performed at 20 °C.

Differential Scanning Calorimetry—Measurements were performed using a MicroCal MCS-DSC instrument as detailed (17). Samples (~3 mg/ml) were dialyzed overnight against 30 mM Mops, pH 7.5. Thermograms of the isolated domains and for reversibility tests were recorded in the presence of 0.5 M 3-(1-pyridinio)-1-propanesulfonate to delay aggregation. Thermograms were analyzed according to a non-two-state model in which the T_m, the calorimetric enthalpy (ΔH_{cal}), and the van't Hoff enthalpy (ΔH_{vH}) of individual transitions are fitted independently using the MicroCal Origin software (version 2.9). The magnitude and source of the errors in the T_m and enthalpy values have been discussed elsewhere (18). Fitting standard errors on a series of three DSC measurements made under the same conditions in the present study were found to be ±0.1 K on T_m and ±1% on both enthalpies. Fitting standard errors on four batches of purified *Ps*PGK were found to be ± 1 K on T_m and ± 10% on both enthalpies.

RESULTS

General Properties—The thermogram of *Ps*PGK (Fig. 1*a*) shows that its heat-induced unfolding is characterized by two distinct heat absorption peaks separated by a temperature interval of about 10 °C (TABLE ONE) and henceforward referred to as the heat-labile (T_m = 49.8 °C) and the heat-stable (T_m = 60.6 °C) transitions (with T_m, the melting point at the top of the transition). In our experimental conditions, no aggregation occurred in the heated sample and a stable post-transition baseline was recorded allowing the calculation of a progress baseline accounting for both transitions (Fig. 1*a*). On this basis, an estimation of the heat capacity difference between the unfolded and the native states can be made for the whole molecule (ΔC_p = 7.47 kcal mol^{-1} K^{-1}), for the heat-labile (ΔC_p = 5,93 kcal mol^{-1} K^{-1}) and the heat-stable (ΔC_p = 1,54 kcal mol^{-1} K^{-1}) transitions. A ΔC_p value of 7.5 kcal mol^{-1} K^{-1} has been reported for yeast PGK (11), and the specific value of 19.3 cal/mol residue for *Ps*PGK (386 amino acid residues) is in perfect agreement with data reported for large proteins (17). As far as heat absorption during unfolding is concerned, the normalized surface (ΔH_{cal}, corre-

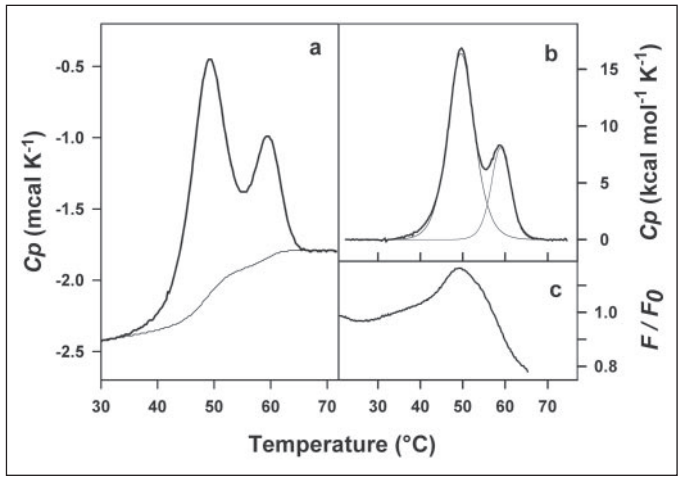

FIGURE 1. **General properties of *Ps*PGK.** *a*, raw thermogram showing the heat-labile and the heat-stable DSC transitions. *b*, normalized and base line-subtracted thermogram showing the deconvolution into two transitions. *c*, heat-induced unfolding recorded by fluorescence showing the dequenching of Trp^{305} around 50 °C.

TABLE ONE

Thermodynamic parameters of the free and liganded *Ps*PGK and of its isolated domains

$\sum\Delta H_{cal}$ is the integrated area of the transition and may differ from the sum of the individual ΔH_{cal} obtained by deconvolution.

Protein and ligand	T_m1	$\Delta H_{cal}1$	$\Delta H_{vH}1$	T_m2	$\Delta H_{cal}2$	$\Delta H_{vH}2$	$\Sigma\Delta H_{cal}$
	°C	kcal mol^{-1}	kcal mol^{-1}	°C	kcal mol^{-1}	kcal mol^{-1}	kcal mol^{-1}
Free *Ps*PGK	49.8	160	98	60.6	57	147	217
+ 5 mM ADP	54.4	165	102	60.9	63	139	226
+ 5 mM 3-PGA	55.1	161	112	60.8	53	158	212
+5 mM Mg^{2+}-ADP, 3-PGA (closed)				60.5	220	250	219
+40 mM Na_2SO_4				56.3	228	154	222
Free N-domain	51.6	11	6				11
Free C-domain				58.3	48	141	48
+5 mM Mg^{2+}-ADP				60.4	96	152	99

sponding to all enthalpy-driven interactions disrupted during unfolding) below the heat-labile transition is nearly twice that of the heat-stable transition (Fig. 1*b*; TABLE ONE), indicating that a large fraction of the native *Ps*PGK conformation has a low stability. As shown in Fig. 2, thermal unfolding of the heat-labile transition is fully reversible. In addition, the $\Delta H_{cal}/\Delta H_{vH}$ ratio for this transition (where ΔH_{vH} is the van't Hoff enthalpy calculated from the slope of the transition) is ~1.5, indicating that the heat-labile transition may be composed by more than one cooperative unit, as confirmed below. By contrast, thermal unfolding of the heat-stable transition is not reversible and, as a result, the $\Delta H_{cal}/\Delta H_{vH}$ ratio decreases to ~0.35. It should be noted that unfolding of the latter transition drastically reduces the reversibility of the heat-labile transition (Fig. 2). This suggests that the protein regions involved in both transitions are structurally connected. Addition of 5 mM dithiothreitol does not improve the reversibility, indicating that oxidation of the three free cysteines (Cys^{56}, Cys^{132}, and Cys^{207}) is not a major determinant of the irreversible unfolding.

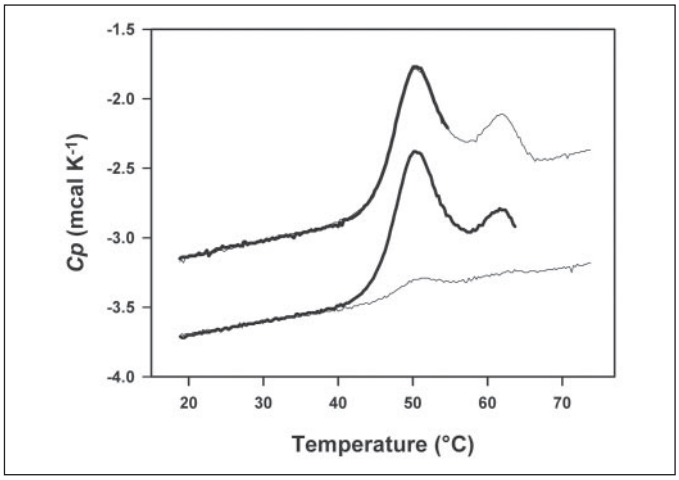

FIGURE 2. **Unfolding reversibility analyzed by DSC.** A first scan was interrupted after the first or the second transition (*thick lines*). Following cooling of the sample in the microcalorimeter cell, a second uninterrupted scan was generated (*thin lines*). The first transition displays a full reversibility, whereas unfolding of the second transition is irreversible.

*Mutagenesis Study of the Structural Domains—Ps*PGK contains one single Trp residue at position 305 in the C-domain. As shown by heat-induced unfolding monitored by fluorescence (excitation wavelength: 295 nm), this Trp is quenched in its microenvironment. Indeed, unfolding results in fluorescence increase (Fig. 1*c*) and the appearance of a hyperfluorescent intermediate. The temperature of maximal dequenching closely corresponds to the melting point of the heat-labile transition observed by DSC. The mutation $Trp^{305} \rightarrow Phe$ totally abolishes the dequenching transition (data not shown) therefore ascertaining the assignment of the fluorescence signal to Trp^{305}. Interestingly, the DSC thermogram of this mutant displays an altered heat-labile transition (Fig. 3), as indicated by the decrease of T_m (−5 °C) and of ΔH_{cal} (−30%), whereas the heat-stable transition remains almost unaffected. One can conclude that the C-domain mainly contributes to the heat-labile transition. On the other hand, the mutation $Phe^{135} \rightarrow Trp$ has been introduced in the N-domain and the DSC trace of this mutant (Fig. 3) also exhibits a drastic destabilization of the heat-labile transition (T_m −8 °C, ΔH_{cal} −50%). These results indicate that both N and C structural domains of *Ps*PGK contribute to the heat-labile DSC transition. Accordingly, each DSC transition of *Ps*PGK cannot be assigned to the unfolding of a specific structural domain. One can also note a slight increase of the T_m for the heat-stable transition in both mutants. This can be tentatively related to the relaxation of weak interactions between interacting domains in the protein when one of these domains is destabilized (9, 11).

When both mutations are combined in the double mutant $Phe^{135} \rightarrow Trp/Trp^{305} \rightarrow Phe$, it is expressed and purified as an inactive and partly folded protein, as demonstrated by the weak DSC heat

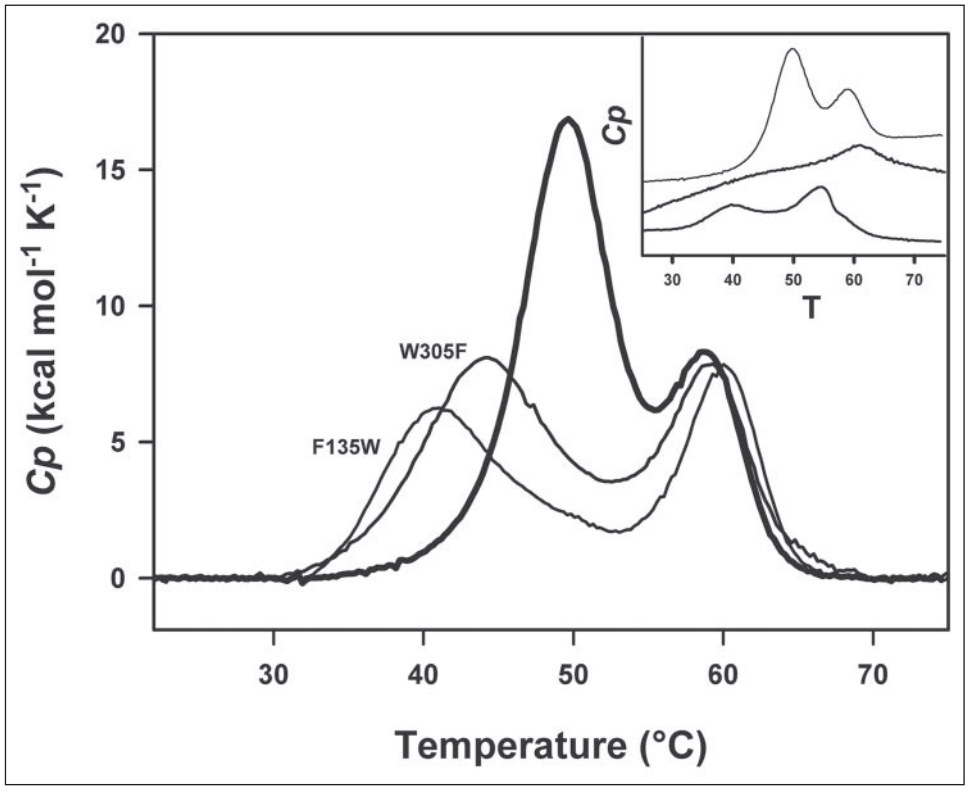

FIGURE 3. **Effects of mutations on the DSC profiles.** Normalized thermograms of *Ps*PGK (*thick line*) and of the mutants $Trp^{305} \rightarrow Phe$ and $Phe^{135} \rightarrow Trp$ illustrating the destabilization of the heat-labile transition resulting from mutations introduced in the N or C structural domains. *Inset* (from the *top*), raw thermograms of *Ps*PGK, of the double mutant $Phe^{135} \rightarrow Trp/Trp^{305} \rightarrow Phe$ and of the double mutant with 20 mM sulfate.

absorption peak (Fig. 3, *inset*). It was found that after addition of 20 mM sulfate ions, the double mutant recovered 20% of the wild-type *Ps*PGK activity. In the presence of sulfate, the DSC thermogram of the mutant exhibits two slight transitions (Fig. 3, *inset*). This indicates that the sulfate ion behaves like a folding effector of *Ps*PGK.

The Isolated N and C Structural Domains—To further characterize the contribution of the *Ps*PGK structural domains in both DSC transitions, the isolated N- and C-domains were expressed in *E. coli* from the *pgk* gene truncated in the middle of the first hinge helix. The plasmid construct coding for the N-domain contained the nucleotide sequence from Met-Thr^{1} to Leu^{170} (mature protein numbering; 18,107.9 Da for 170 aa), whereas the sequence for Met-Thr^{1}–Ala^{172} to Ala^{386} was used for the C-domain (21,996.3 Da for 216 aa). It should be recalled that because the C-terminal end of PGK folds into the N-domain, truncation in the middle of the gene results in the expression of an N-domain devoid of ~15 residues that remain attached to the recombinant C-domain. N-terminal amino acid sequencing and mass spectrometry analyses (N-domain: 18,107 Da; C-domain: 21,999 Da) indicated that the initiating formylmethionine has been removed and that no other post-translational modification occurred during the expression and purification processes.

The UV absorbance spectra well reflect the aromatic amino acid content of the analyzed proteins. The N-domain (six Phe, three Tyr) lacking Trp has a low absorption coefficient ($\epsilon_{280\ nm}$ = 3,960 M^{-1} cm^{-1}) and its spectrum is dominated by Tyr residues, with three slight shoulders from Phe between 260 and 270 nm (Fig. 4*a*). Having an additional Trp residue, the absorption coefficient of the C-domain (nine Phe, three Tyr, one Trp) is much higher ($\epsilon_{280\ nm}$ = 9,530 M^{-1} cm^{-1}). An equimolar mix of both N- and C-domains restores the absorbance value of the native *Ps*PGK but the imperfect superimposition of the spectra indicates slight differences in the aromatic microenvironment within the recombinant domains. The fluorescence emission spectrum of *Ps*PGK (Fig. 4*b*) is poorly defined as a result of the above-mentioned quenching of Trp305. Similarly, the N-domain fluorescence spectrum is dominated by Tyr residues. However, the pronounced red shift of the C-domain fluorescence spectrum shows that Trp 305 is dequenched and therefore, this residue is not in its native microenvironment in the recombinant domain. It follows that the equimolar mix of both domains restores the maximal fluorescence intensity of the native *Ps*PGK but at a higher emission wavelength. The far-UV circular dichroism spectrum of the native *Ps*PGK (Fig. 4*c*) displays two strong ellipticity minima at 208 and 222 nm indicating a high content of secondary structures. The spectra of both isolated N- and C-domains also present these minima but at a weaker ellipticity, especially for the N-domain. As a result, the equimolar mix of both domains reveals a lower secondary structure content as compared with the native enzyme. Finally, the near-UV CD spectra indicate an asymmetric environment of aromatic residues (and possibly of cysteines) typical of a folded conformation in the three proteins and the equimolar mix (Fig. 4*d*). From these spectrophotometric analyses, it can be concluded that the isolated N- and C-domains possess well organized secondary structures and a defined tertiary structure which however differ from the native state of *Ps*PGK.

Nevertheless, the DSC thermograms of these isolated domains reveal their individual contribution to the biphasic profile of the native *Ps*PGK (Fig. 5). The recombinant C-domain unfolds at a temperature closely corresponding to the heat-stable transition and accounts for about 80% of heat absorption (ΔH_{cal} = 48 kcal mol^{-1}). By contrast, the N-domain is strongly destabilized and only accounts for less than 10% (ΔH_{cal} = 11 kcal mol^{-1}) of the heat-labile transition. It seems therefore that only the C-domain contributes to the heat-stable DSC transition, whereas the

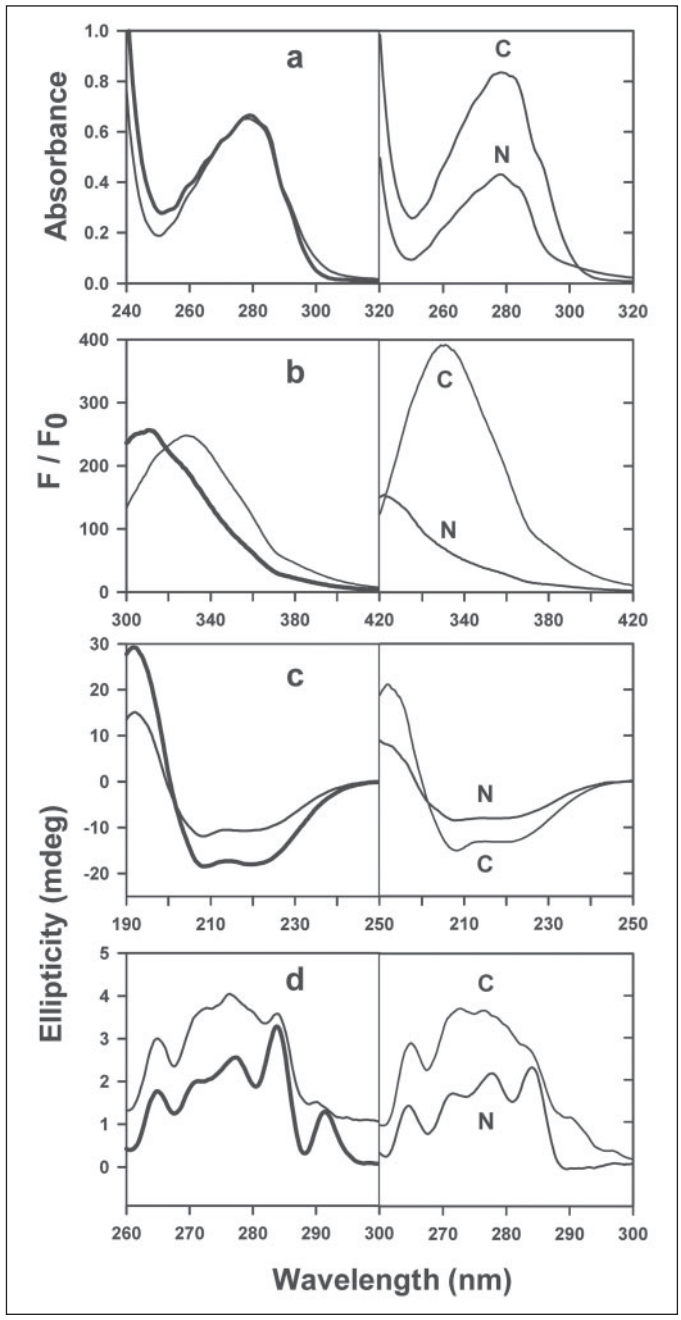

FIGURE 4. **Spectroscopic properties of *Ps*PGK and of its isolated domains.** *a–d*, UV absorbance (*a*), intrinsic fluorescence emission (*b*), far-UV (*c*), and near-UV (*d*) circular dichroism spectra. *Right panels*, isolated N- and C-domains; *left panels*, native *Ps*PGK (*thick lines*) and equimolar mix of the isolated N- and C-domains. Protein concentrations are identical, *i.e.* absorbance 2 mg/ml; fluorescence 0.25 mg/ml; far-UV CD 0.2 mg/ml; near-UV CD 2 mg/ml. Buffer is 50 mM Tris, 5 mM dithiothreitol, 0.5 mM EDTA, pH 7.5, except for far-UV CD (10 mM Na_2HPO_4, pH 7.5).

structures of both domains responsible for the heat-labile DSC transition have not a compact conformation in the recombinant fragments. The spectroscopic and calorimetric data therefore indicate that the heat-labile structures in the recombinant domains tend to have molten globule-like properties, *i.e.* a defined but non-compact conformation with a low intrinsic conformational stability (Figs. 4 and 5). This contrasts with the well folded isolated domains obtained from more stable PGKs (10, 19, 20).

Interestingly, the isolated C-domain still binds the substrate Mg^{2+}-ADP (Fig. 5, *inset*, and TABLE ONE), as revealed by the large (ΔH_{cal} +50

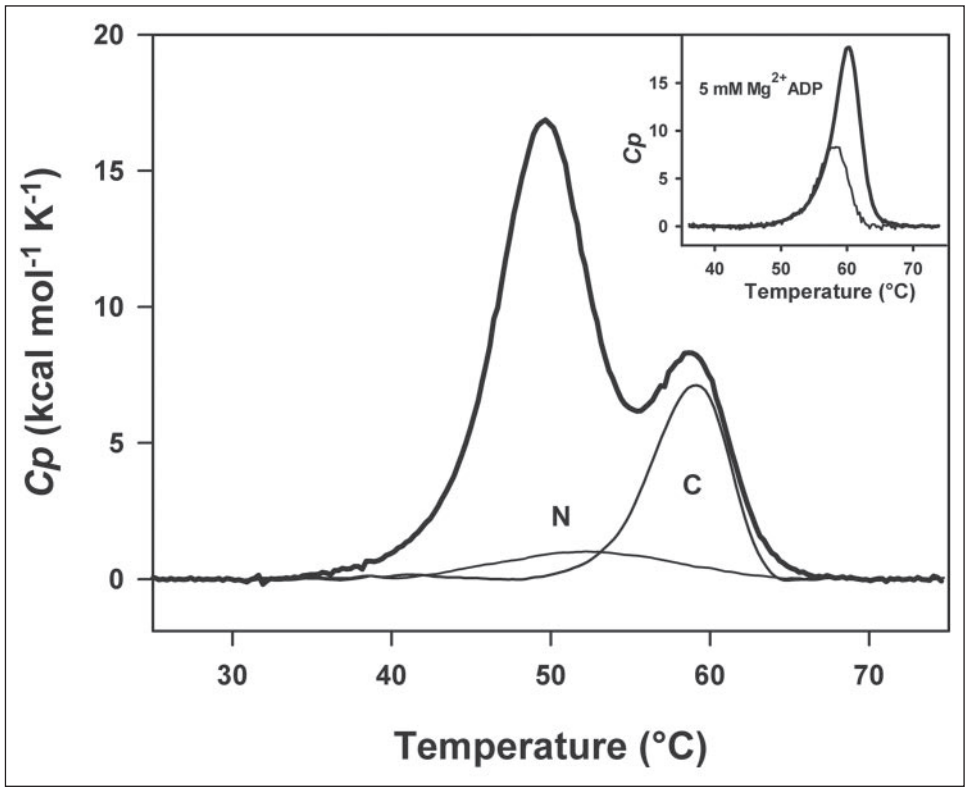

FIGURE 5. **Normalized thermograms of *Ps*PGK (*thick line*) and of its isolated N- and C-domains.** *Inset*, thermograms of the unliganded (*thin line*) and of the substrate-bound (*thick line*) isolated C-domain.

kcal mol^{-1}) and sharp transition at a higher T_m (+2 °C). On the other hand, both 3-PGA and sulfate seem to bind to the isolated N-domain, but these effects cannot be quantified as a result of the weakness of the heat absorption peak.

Substrate-induced Stability Changes—Crystallographic studies have shown that the PGK from *Trypanosoma brucei* can be trapped in the closed, active conformation (7) upon incubation with one substrate (Mg^{2+}-ADP) and one product (3-PGA). In these conditions, the DSC thermogram of *Ps*PGK (Fig. 6) reveals that substrate binding and the resulting hinge-bending motions drive the free (open) *Ps*PGK into a closed, compact and uniformly more stable conformation, as indicated by the single sharp transition at a higher T_m. The $\Delta H_{cal}/\Delta H_{vH}$ ratio of ~0.9 also indicates that unfolding of the closed conformation is cooperative and approaches a two-state mechanism which however is poorly reversible (~6%; data not shown). The nonhydrolyzable nucleotide analog AMP-pnp has been used to study hinge bending but the crystal structures of the porcine 3-PGA-AMP-pnp (21) and the yeast 3-PGA-AMP-pnp (22) complexes do not adopt a closed conformation. As a matter of fact, the thermogram of *Ps*PGK incubated with Mg^{2+} AMP-pnp and 3-PGA (Fig. 6) is indicative of a less compact and stable conformation (estimated from the sharpness and *Tm* of the transition, respectively) than that recorded for the closed conformation. It should also be noted that in the absence of Mg^{2+}, the conformational changes promoted by ADP and 3-PGA are less pronounced (Fig. 6), underlining that the true physiological substrate is the complex Mg^{2+}-ADP.

Crystallographic studies have shown that the individual substrates do not induce the closed conformation (5, 6). However, the DSC thermograms of *Ps*PGK incubated with one substrate (Fig. 6) display drastic alterations of both the heat-labile and heat-stable transitions, revealing significant modifications of the structure energetics. Finally, the DSC traces of *Ps*PGK in the presence of Mg^{2+}-ADP and of Mg^{2+}-ATP are markedly different suggesting that upon phosphoryl transfer to ATP, the enzyme undergoes a noticeable conformational change. It should be

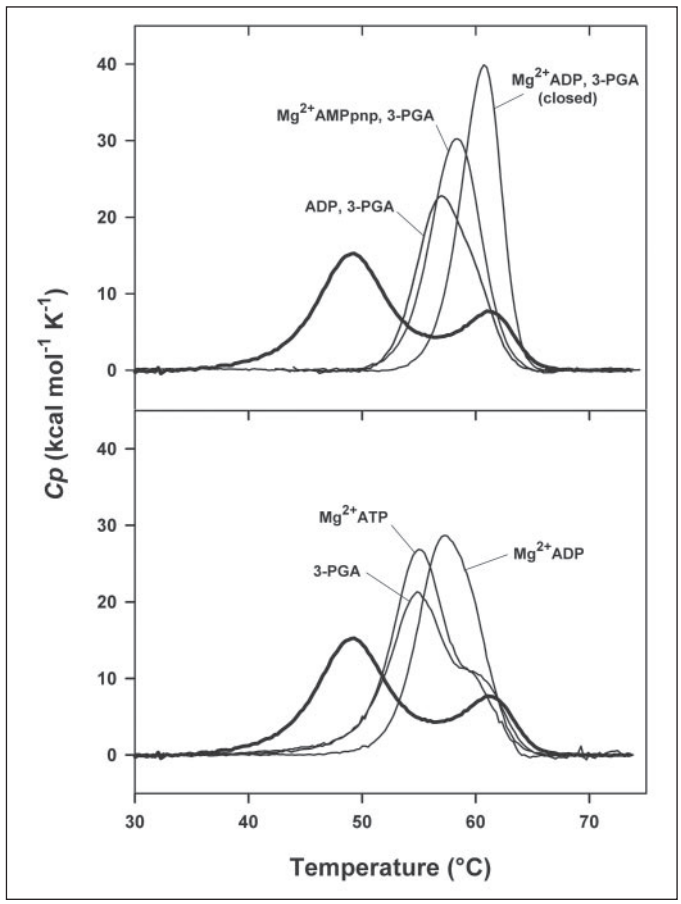

FIGURE 6. **Substrate-induced stability changes of *Ps*PGK.** Normalized thermograms of the free enzyme (*thick lines*) and of the substrate-bound enzyme (*thin lines*). The concentration of each substrate was 5 mM.

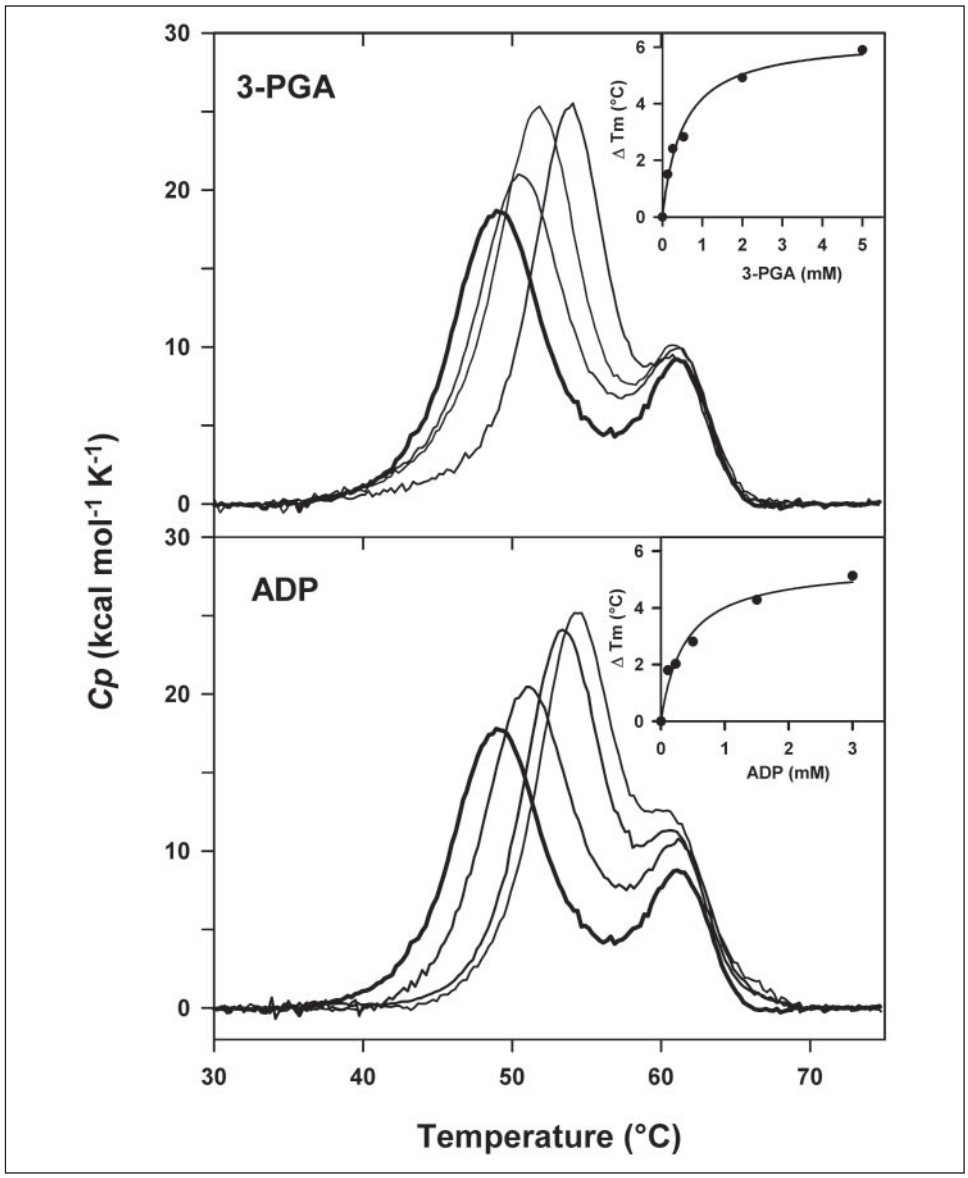

FIGURE 7. **Effect of the triose and nucleotide substrates on *Ps*PGK thermograms. The free enzyme (***thick lines***)** and increasing concentration of 3-PGA (0.13, 0.53, and 2.0 mM) or ADP (0.23, 1.5, and 3 mM). *Insets*, plots of T_m for the heat-labile transition at increasing substrate concentrations; the *solid line* is a non-linear regression fit for a binding isotherm.

noted that all these substrate-induced stability changes only affect the T_m values and the unfolding cooperativity of the transitions. Indeed, as shown in TABLE ONE, there is no significant variation of the surface of the transitions (ΔH_{cal}) for the binary and ternary *Ps*PGK complexes, whereas the sharpness (ΔH_{vH}) and T_m of the transitions are modified.

Substrate and Ion Binding—The available crystal structures of binary and ternary PGK complexes and a multiple sequence alignment allowed to identify the highly conserved residues of *Ps*PGK involved in substrate and ion binding. 3-PGA binds to the N-terminal domain (residues Asp^{20}, Asn^{22}, Arg^{35}, His^{58}, Arg^{61}, Arg^{112}, Gly^{141}, Arg^{145}, Gly^{362}, Gly^{363}, and Ala^{364}) in the so-called basic patch, whereas ADP binds to the C-terminal domain (residues Ser^{191}, Lys^{196}, Ile^{282}, Leu^{283}, Asn^{306}, Glu^{313}, Gly^{340}, and Thr^{342}). Fig. 7 shows the effect of increasing concentrations of both substrates on the DSC thermograms of *Ps*PGK. It can be seen that upon 3-PGA binding, the T_m of the heat labile transition is displaced toward higher values whereas the heat-stable transition remains unaffected. This confirms that the structural N-domain bearing the 3-PGA binding site belongs to the heat-labile DSC transition. On the other hand, upon ADP binding the stability of the heat-labile transition is improved, but in this case, the surface (ΔH_{cal}) of the heat-stable transition is also increased. This again confirms that the structural C-domain bearing the ADP binding site contributes to both the heat-labile and heat-stable DSC transitions. Interestingly, a plot of the T_m increase for the heat-labile transition as a function of the substrate concentration can be fitted to a binding isotherm (Fig. 7, *insets*) providing apparent K_d values of 0.51 mM for 3-PGA and 0.38 mM for ADP. These values are in agreement with the K_m values previously determined by standard kinetic methods (14).

The above-mentioned experiments have been performed in the absence of Mg^{2+}. This ion was shown to interact with an acidic side chain of the ADP binding site (7), corresponding to Asp^{341} in the C-domain of *Ps*PGK. Fig. 8 shows that increasing concentrations of $MgCl_2$ only affect the heat-stable DSC transition by decreasing its T_m. At $MgCl_2$ concentrations higher than 2 mM, the heat-stable transition tends to fuse with the heat-labile DSC transition that remains unaltered but sample precipitation precluded further analysis of this phenomenon. These results clearly demonstrate that the Mg^{2+}-binding site belongs to the heat-stable DSC transition. Finally, the sulfate ion can be viewed as a test case for our assignment of the DSC transitions because it has been reported to bind both to the N- (Arg^{61}) and C- (Lys^{192})

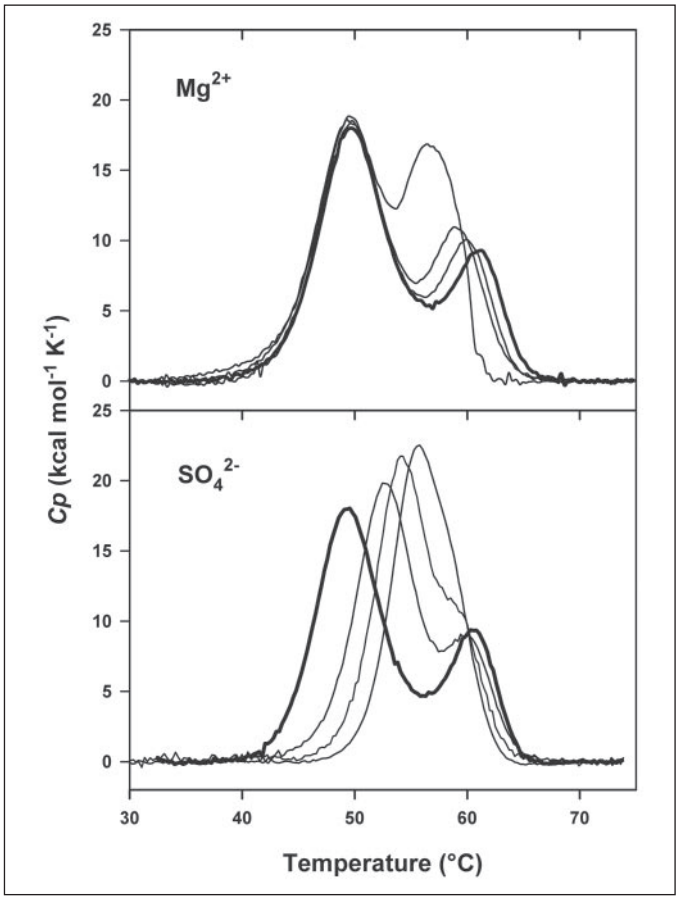

FIGURE 8. **Effect of the co-substrate cation and of the activator anion on *Ps*PGK thermograms.** The free enzyme (*thick lines*) and increasing concentration of $MgCl_2$ (0.5, 1, and 3 mM) or Na_2SO_4 (10, 20, and 40 mM).

domains (23). And indeed, increasing Na_2SO_4 concentrations affect both the heat-labile and heat-stable DSC transitions (Fig. 8), which fuse in a conformation mimicking the substrate-induced closed conformation, however, at a lower T_m.

DISCUSSION

Stability and Structural Domains—Several multidomain proteins display distinct stability domains resulting in multiphasic DSC thermograms (24). In some cases, a close correlation was found between structural and stability domains, *i.e.* each DSC transition can be assigned to the unfolding of a specific structural domain (25–29). However, *Ps*PGK clearly demonstrates that such correlation is not always valid as, in this case, we have shown that the heat-stable DSC domain belongs to the structural C-domain, whereas both N and C structural domains contribute to the main heat-labile DSC domain. The size of the heat-stable domain in *Ps*PGK can be estimated to 100 residues in a first approximation, assuming that all 386 residues contribute equally to ΔH_{cal} of the DSC transitions (TABLE ONE). A more precise estimation of 80 residues can be based on ΔC_p of the transitions (5.93 and 1.54 kcal mol^{-1} K^{-1} for the first and second transitions, respectively) because this parameter has been found relatively constant for proteins of similar size, whatever their intrinsic stability (17). The spectroscopic and mutagenesis studies as well as the effects of substrates and ions on the DSC transitions indicate that this heat-stable domain includes or is very close to the nucleotide binding site. If the stability pattern of the *Ps*PGK structural C-domain (*i.e.* containing both heat-labile and heat-stable structures) is extended to other homologous PGK, this can partly explain the contradicting results reported for the stability of the C-domain (9–13).

Substrate-induced Stability Changes and Hinge-bending Motions—Considering the weak stability of the major DSC transition (Fig. 1), the free *Ps*PGK appears to possess a relatively loose open conformation. Upon binding of a single substrate molecule, either Mg^{2+}ADP or 3-PGA, the heat-labile structures evolve toward a more compact conformation (Fig. 7). This can be related to an induced-fit mechanism by which binding of the substrate induces a structural rearrangement of the binding site. It should be noted that this drastic modification of *Ps*PGK conformational stability mainly involves the structure energetics because only discrete modifications have been reported between the crystal structures of free and single substrate-bound PGKs (5, 6). The behavior of the isolated C-domain provides useful insights into the energetics of hinge-bending motions in *Ps*PGK. Indeed, Fig. 5 (*inset*) and TABLE ONE show a drastic increase of ΔH_{cal} and of T_m for this isolated domain upon Mg^{2+}-ADP binding. An estimation of the conformational stability in the free and substrate-bound states can be obtained using Equation 1.

$$\Delta G(T) = \Delta H_{cal}(1 - T/T_m) + \Delta C_p(T - T_m) - T\Delta C_p \ln T/T_m) \quad \text{(Eq. 1)}$$

The validity of this approximation has been discussed elsewhere (30–32). The computed stability curves indicate an increase of the conformational stability (free energy of unfolding) of 5.5 kcal mol^{-1} upon substrate binding. On the other hand, the free energy of substrate binding can be estimated to -5 kcal mol^{-1} using the K_m value for the nucleotide (0.21 mM) and the following relation (Equation 2).

$$\Delta G_b = -RT \ln K_a \quad \text{(Eq. 2)}$$

Comparison of both free energy estimates strongly suggests that the nucleotide binding free energy is transferred into conformational stability. However, such behavior of the heat-stable transition is not observed in the native *Ps*PGK upon ADP (Fig. 7) and Mg^{2+} (Fig. 8) binding. One can therefore propose that in the native enzyme, the gain in conformational stability arising from substrate binding is now converted into the energy required for hinge-bending motions and domain closure. The lack of $\Sigma\Delta H_{cal}$ difference between the free and closed forms of *Ps*PGK (TABLE ONE) also supports this view. Finally, in a thoughtful study of PGK activation, the authors concluded that it cannot be decided whether anion activation is a consequence of domain closure or anion binding itself mediates the closure by connecting the two domains (23). From our results, it seems that the latter hypothesis is valid, as demonstrated by the apparent domain closure induced by the sulfate anion activator (Fig. 8).

Activity at Low Temperatures—The unusual stability pattern of *Ps*PGK should also be considered in the context of the enzyme adaptations to catalysis at low temperatures. In order to catalyze the essential glycolytic step at temperatures close to 0 °C found in the Antarctic environment, this enzyme possesses a high specific activity to compensate for the reduction of chemical reaction rates at such low temperatures. In addition, *Ps*PGK displays a high affinity for the nucleotide, therefore improving the k_{cat}/K_m ratio which is the relevant parameter for intracellular enzymes (14). It has been argued that the high activity of cold-adapted enzymes is gained through an improved flexibility or mobility of the active site and of the structures bearing the active site residues in order to facilitate molecular motions in low thermal energy conditions (32–34). In the case of *Ps*PGK, the active site is formed by the

interface of the N- and C-domains that have to move to bring the substrates in close proximity. Accordingly, the predominant weak stability of this enzyme can enhance the substrate-induced conformational changes (Figs. 6 and 7) and the resulting hinge-bending motions at low temperatures. It has also been suggested that during the course of evolution, some psychrophilic enzymes have reached a state close to the lowest stability compatible with the native state (17, 33, 35). This is supported here by the drastic effects of the single conservative mutations introduced in both N- and C-domains (Fig. 3), by the almost unfolded state of the double mutant (Fig. 3, inset) and by the lack of compact conformation of the structures forming the heat-labile DSC transition in the isolated domains (Figs. 4 and 5). As far as substrate binding is concerned, most psychrophilic enzymes have a reduced affinity arising from the active site mobility (33, 36), whereas *Ps*PGK has a better affinity for the nucleotide. One can therefore propose that the heat-stable domain of *Ps*PGK provides a more compact and structured nucleotide binding site which, consequently, has a high affinity. This seems to be an elegant molecular adaptation allowing the optimization of both k_{cat} and K_m at low temperatures, not previously observed in other psychrophilic enzymes.

Acknowledgments—We thank R. Marchand and A. Dernier for their skillful technical assistance. The facilities offered by the Institut Polaire Français are also acknowledged. We thank Drs. N. Aghajari and R. Haser (CNRS, Lyon, France) for providing the atomic coordinates of PsPGK before publication.

REFERENCES

1. Jaenicke, R. (1999) *Prog. Biophys. Mol. Biol.* **71,** 155–241
2. Reed, M. A., Hounslow, A. M., Sze, K. H., Barsukov, I. G., Hosszu, L. L., Clarke, A. R., Craven, C. J., and Waltho, J. P. (2003) *J. Mol. Biol.* **330,** 1189–1201
3. Blake, C. C., and Evans, P. R. (1974) *J. Mol. Biol.* **84,** 585–601
4. Watson, H. C., Walker, N. P., Shaw, P. J., Bryant, T. N., Wendell, P. L., Fothergill, L. A., Perkins, R. E., Conroy, S. C., Dobson, M. J., Tuite, M. F., Kingsman, A. J., and Kingsman, S. M. (1982) *EMBO J.* **1,** 1635–1640
5. Harlos, K., Vas, M., and Blake, C. F. (1992) *Proteins* **12,** 133–144
6. Davies, G. J., Gamblin, S. J., Littlechild, J. A., Dauter, Z., Wilson, K. S., and Watson, H. C. (1994) *Acta Crystallogr. Sect. D Biol. Crystallogr.* **50,** 202–209
7. Bernstein, B. E., Michels, P. A., and Hol, W. G. (1997) *Nature* **385,** 275–278
8. Bernstein, B. E., and Hol, W. G. (1998) *Biochemistry* **37,** 4429–4436
9. Brandts, J. F., Hu, C. Q., Lin, L. N., and Mas, M. T. (1989) *Biochemistry* **28,** 8588–8596
10. Missiakas, D., Betton, J. M., Minard, P., and Yon, J. M. (1990) *Biochemistry* **29,** 8683–8689
11. Freire, E., Murphy, K. P., Sanchez-Ruiz, J. M., Galisteo, M. L., and Privalov, P. L. (1992) *Biochemistry* **31,** 250–256
12. Gast, K., Damaschun, G., Desmadril, M., Minard, P., Muller-Frohne, M., Pfeil, W., and Zirwer, D. (1995) *FEBS Lett.* **358,** 247–250
13. Sherman, M. A., Beechem, J. M., and Mas, M. T. (1995) *Biochemistry* **34,** 13934–13942
14. Bentahir, M., Feller, G., Aittaleb, M., Lamotte-Brasseur, J., Himri, T., Chessa, J. P., and Gerday, C. (2000) *J. Biol. Chem.* **275,** 11147–11153
15. Mandelman, D., Bentahir, M., Feller, G., Gerday, C., and Haser, R. (2001) *Acta Crystallogr. Sect. D Biol. Crystallogr.* **57,** 1666–1668
16. Feller, G., Bussy, O., Houssier, C., and Gerday, C. (1996) *J. Biol. Chem.* **271,** 23836–23841
17. Feller, G., d'Amico, D., and Gerday, C. (1999) *Biochemistry* **38,** 4613–4619
18. Matouschek, A., Matthews, J. M., Johnson, C. M., and Fersht, A. R. (1994) *Protein Eng.* **7,** 1089–1095
19. Hosszu, L. L., Craven, C. J., Spencer, J., Parker, M. J., Clarke, A. R., Kelly, M., and Waltho, J. P. (1997) *Biochemistry* **36,** 333–340
20. Zaiss, K., and Jaenicke, R. (1999) *Biochemistry* **38,** 4633–4639
21. May, A., Vas, M., Harlos, K., and Blake, C. (1996) *Proteins* **24,** 292–303
22. McPhillips, T. M., Hsu, B. T., Sherman, M. A., Mas, M. T., and Rees, D. C. (1996) *Biochemistry* **35,** 4118–4127
23. Szilagyi, A. N., and Vas, M. (1998) *Biochemistry* **37,** 8551–8563
24. Privalov, P. L. (1982) *Adv. Protein Chem.* **35,** 1–104
25. Novokhatny, V. V., Kudinov, S. A., and Privalov, P. L. (1984) *J. Mol. Biol.* **179,** 215–232
26. Tatunashvili, L. V., Filimonov, V. V., Privalov, P. L., Metsis, M. L., Koteliansky, V. E., Ingham, K. C., and Medved, L. V. (1990) *J. Mol. Biol.* **211,** 161–169
27. Lin, L. N., Mason, A. B., Woodworth, R. C., and Brandts, J. F. (1994) *Biochemistry* **33,** 1881–1888
28. Misselwitz, R., Welfle, K., and Welfle, H. (1994) *Int. J. Biol. Macromol.* **16,** 187–194
29. Suzuki, Y., Takano, K., and Kanaya, S. (2005) *FEBS J.* **272,** 632–642
30. Privalov, P. L., and Medved, L. V. (1982) *J. Mol. Biol.* **159,** 665–683
31. Vogl, T., Jatzke, C., Hinz, H. J., Benz, J., and Huber, R. (1997) *Biochemistry* **36,** 1657–1668
32. D'Amico, S., Marx, J. C., Gerday, C., and Feller, G. (2003) *J. Biol. Chem.* **278,** 7891–7896
33. Feller, G., and Gerday, C. (2003) *Nat. Rev. Microbiol.* **1,** 200–208
34. Georlette, D., Blaise, V., Collins, T., D'Amico, S., Gratia, E., Hoyoux, A., Marx, J. C., Sonan, G., Feller, G., and Gerday, C. (2004) *FEMS Microbiol. Rev.* **28,** 25–42
35. D'Amico, S., Gerday, C., and Feller, G. (2001) *J. Biol. Chem.* **276,** 25791–25796
36. Xu, Y., Feller, G., Gerday, C., and Glansdorff, N. (2003) *J. Bacteriol.* **185,** 2161–2168